ELSEVIER

Engineering Structures 24 (2002) 671–685

ENGINEERING STRUCTURES

www.elsevier.com/locate/engstruct

Linear dynamics of tensegrity structures

Cornel Sultan [a,*], Martin Corless [b], Robert E. Skelton [c]

[a] *Harvard University, Boston, MA 02115, USA*
[b] *Purdue University, West Lafayette, IN 47907-1282, USA*
[c] *University of California, La Jolla, CA 92093-0411, USA*

Received 11 December 2000; received in revised form 10 August 2001; accepted 24 September 2001

Abstract

The linearized equations of motion for tensegrity structures around arbitrary equilibrium configurations are derived. For certain tensegrity structures which yield particular equilibrium configurations of practical interest, the linearized models of their dynamics around these configurations are presented. Evidence which indicates that these equilibria are stable is given and some stiffness and dynamic properties of these structures are investigated. © 2002 Elsevier Science Ltd. All rights reserved.

Keywords: Tensegrity structures; Dynamics; Vibration; Damping

1. Introduction

Since their introduction by Snelson, Fuller and Emmerich around 1948, tensegrity structures have been a matter of surprise and fascination. Their ability to maintain an equilibrium shape under no external force (a property of tensegrity structures called prestressability), their flexibility achieved through an ingenious design which combines rigid elements and elastic tendons, and their very low weight, aroused the interest of artists, scientists, and engineers.

Several documents show that patents for tensegrity structures were applied for, almost simultaneously, by R.B. Fuller in the US and by D.G. Emmerich in France. What happened afterwards was a source of controversy between Snelson, Fuller and Emmerich regarding the priority of the invention (interested readers are referred to articles published in the International Journal of Space Structures 11(1–2), 1996). It should be emphasized that the structural system described by the three authors is the same: a simple structure comprising three struts and nine tendons. The tensegrity concept was later generalized by other researchers [1–7].

Tensegrity structures are lattices that form spatial networks depending on the arrangement of the vertices: tower-like structures, layered networks, or crystalline type networks according to the number of directions they develop. They consist of a set of *soft* members (e.g. elastic tendons), and a set of *hard* members (e.g. bars). A perspective view of a tensegrity structure composed of 6 bars and 24 tendons is given in Fig. 1. It is apparent that tensegrity structures are very flexible, being capable of large displacement; their shape can be easily changed by modifying the tendons lengths.

In tensegrity structures research, more attention has been paid so far to the statics of these structures than to their dynamics. Due to substantial contributions by various researchers [3,8,2,9–15,7,16,17] tensegrity statics research has reached a certain stage of maturity, whereas these structures dynamics is still an emerging field. It is our strong conviction that research in tensegrity structures should focus considerably more on their dynamics and control. This is so because tensegrity structures are excellent candidates for controllable structures, with the actuators and sensors easily embedded in the structures (for example the tendons can carry both actuating and sensing functions). Future applications of tensegrity structures are mostly in the field of controllable structures capable of large motions, which would exploit these structures flexibility and versatility: deployable structures, robotic arms, space telescopes, motion simulators, etc. These applications development is not possible without thorough investigation and understanding of tensegrity structures dynamics.

* Corresponding author. Tel.: +1-617-381-0013.
E-mail address: cornel.sultan@tch.harvard.edu (C. Sultan).

PII: S0141-0296(01)00130-4

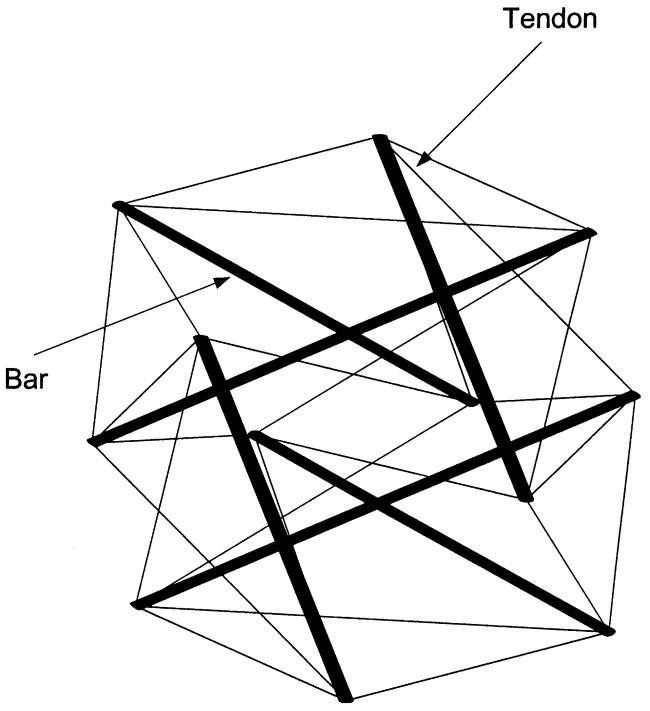

Fig. 1. A tensegrity structure.

Very few articles on tensegrity structures dynamics have been published so far. Motro [11] presents some results of a linear dynamics experimental analysis of a tensegrity structure composed of three bars and nine tendons. The experiment determines the dynamic characteristics of the structure by harmonic excitation of a node and measurement of the responses of the other nodes. In another article, Furuya [18] analyzes the vibrational characteristics of some tensegrity structures using finite element programs and concludes that the modal frequencies increase as the pretension increases. Murakami [19–21] uses the Lagrangian and Eulerian approach to derive the equations of motion of a large class of structures and applies it to some tensegrity structures for numerical simulations and modal analysis. Recently Oppenheim and Williams [22] tackled the dynamics of tensegrity structures analytically. In their article the dynamics of a tensegrity structure composed of three bars and six tendons is examined showing that, if only linear kinetic damping in the tendons is assumed, the geometric flexibility of the structure leads to a much slower rate of decay of vibrations than might be expected. In order to improve the structure's damping properties, linear kinetic damping of the angular motion between structural members in contact is assumed, leading to an exponential rate of decay. In another article by Oppenheim and Williams [23] these remarks are reinforced leading to the conclusion that friction in the rotational joints of the structure is a more important source of damping than the damping in the tendons.

Sultan [16] derives mathematical models of the nonlinear dynamics for a large class of tensegrity structures. The resulting equations are second order ordinary differential ones, illustrating an important advantage of these structures: their behavior can be described accurately enough by ordinary differential equations, which are much easier to deal with than partial differential equations, usually used to analyze classical (truss) flexible structures.

In the area of active control the published literature is sparse. Djouadi [24] presents a tensegrity antenna for which a quadratic optimal controller to minimize the nodal displacements is designed. Sultan [25] simultaneously designs the control system and a tensegrity structure, showing that the resulting system has better performance than if the sequential approach (structure design followed by controller design) is applied. In a series of articles, Sultan, Corless and Skelton propose and investigate various applications of tensegrity structures in motion simulators (see Sultan [6,26]), deployable structures [27], sensors [28], or space telescopes [29].

In this article we present linearized models of the dynamics of a class of tensegrity structures around reference solutions of the nonlinear equations of motion. Some particular tensegrity structures are then studied; the reference solutions are equilibrium ones, previously investigated by Sultan [7]. Explicit expressions of the linearized models matrices are given. Using these models, conclusions about some important properties of the structures investigated (stability of the corresponding equilibrium configurations, stiffness, etc.) are drawn.

2. Linearized dynamics of tensegrity structures

In the following we present some results on nonlinear equations of motion of a class of tensegrity structures derived by Sultan [16] then we present the corresponding linearized equations of motion.

Consider a tensegrity structure composed of *E elastic* and *massless* tendons and *R rigid* bodies. The following mathematical modeling assumptions are made: all constraints on the system are *holonomic*, *scleronomic* and *bilateral*, the external constraint forces are *workless*, the forces exerted on the structure by external force fields (e.g. gravitational) are neglected, the joints of the system are affected at most by *linear kinetic friction* (linear kinetic friction means that the friction forces and torques are proportional to the relative linear and angular velocities between the members in contact), the tendons are at most affected by *linear kinetic damping* (linear kinetic damping means that the damping force introduced by a tendon is proportional to the time derivative of its elongation). Under these assumptions the equations of motion for this system can be derived as shown by Sultan [16] yielding:

$$M(q)\ddot{q} + c(q,\dot{q}) + A(q)T(q) + C(q)\dot{q} + H(q)F \qquad (1)$$

$= 0$

where

- $q = [q_1 \ldots q_N]^T$ is the vector of independent generalized coordinates used to describe the structure's configuration.
- $M(q)$ is the mass matrix.
- $c(q,\dot{q})$ is a vector of quadratic functions in $\dot{q}$, whose components can be expressed as:

$$c_i = \sum_{j=1}^{N}\sum_{n=1}^{N}\left(\frac{\partial M_{ij}}{\partial q_n} - \frac{1}{2}\frac{\partial M_{jn}}{\partial q_i}\right)\dot{q}_j\dot{q}_n,\ i = 1,\ldots,N. \tag{2}$$

  $A(q)T(q)$ is the vector of elastic generalized forces where $A[n,j] = \dfrac{\partial l_j}{\partial q_n}$, $n = 1,\ldots, N, j = 1,\ldots,E$, T_j and l_j being the tension and length, respectively, of tendon j.
- $C(q)\dot{q}$ is a vector of generalized damping forces where $C(q)$ is the damping matrix (we note that this form of generalized damping forces is valid only for the linear kinetic friction and damping assumptions).
- $H(q)F$ is a vector of generalized forces due to external forces and torques where F is the vector of external forces and torques and $H(q)$ is the disturbance matrix. The forces and torques included in F are not conservative or damping ones (e.g. they are external forces acting on the rigid bodies).

We consider that the dynamics of the structure is controlled through tendons. This task can be accomplished by motors attached, for example, to the rigid bodies. These motors work as follows. For example, the motor pulls a tendon and rolls it over a small wheel in such a way that its active length is shortened: the part of the tendon which is rolled over the motor wheel no longer carries force. Hence this control procedure works as if the rest-length of the tendon would be shortened. Similarly, when the motor reverses its direction of rotation, a portion of the inactive tendon becomes active, carrying force; hence the rest-length of the tendon increases. We call this procedure of tendon control, *rest-length control*.

Let q_e denote an equilibrium solution of Eq. (1), that is $\ddot{q}_e = \dot{q}_e = 0$. The linearized equations of motion which describe the approximate dynamics of the structure in the neighborhood of q_e are derived using Taylor series expansion. This yields

$$M_e\ddot{\tilde{q}} + C_e\dot{\tilde{q}} + K_e\tilde{q} + B_e u + H_e f = 0 \tag{3}$$

where

$$\tilde{q} = q - q_e,\ u = l_0 - l_{0_e},\ f = F - F_e$$

and M_e, C_e, K_e, B_e, and H_e are the mass, damping, stiffness, control, and disturbance matrices, respectively, evaluated at q_e.

The control variables are denoted by u, whereas l_{0_c} represents the vector of rest-lengths at equilibrium. The disturbances are denoted by f, F_e being the vector of external forces and torques at equilibrium.

3. Two stage SVD tensegrity structures

In the following we present the linearized equations of motion for a certain class of tensegrity structures, coined *two stage SVD tensegrity structures*. These structures have great opportunities for industrial applications as shown by Sultan [25,27,28]. Their static properties have been thoroughly investigated by Sultan [7,16].

3.1. Description

A two stage SVD tensegrity structure is composed of six bars, labeled $A_{ij}B_{ij}$, $i = 1,2,3$, $j = 1,2$, a rigid top ($B_{12}B_{22}B_{32}$), a rigid base ($A_{11}A_{21}A_{31}$), and 18 tendons (see Figs. 2 and 3). A stage is composed of bars with the same second index (e.g. $A_{11}B_{11}$, $A_{21}B_{21}$, and $A_{31}B_{31}$ belong to the first stage). The acronym 'SVD' comes from the notation we introduce for the tendons: $B_{i1}A_{j2}$ will be called *saddle* tendons, $A_{j1}B_{i1}$ and $A_{j2}B_{i2}$ *vertical* tendons, and $A_{j1}A_{i2}$ and $B_{j1}B_{i2}$ *diagonal* tendons respectively.

The assumptions made for the mathematical modeling of two stage SVD tensegrity structures are: the tendons are *massless, linear elastic*, and *not-damped* (not affected by damping), the base and the top are *rigid* bodies, the bars are *rigid, axially symmetric*, and for each bar the rotational degree of freedom around the longitudinal axis of symmetry is neglected. This is a reasonable assumption if the points of attachment of the bars to the rigid bodies and to the tendons belong to the axes of symmetry of the bars, so that no longitudinal torque is generated, or, if we assume that the thickness of any bar is negligible. *Linear kinetic* friction torques (proportional to the relative angular velocity) act at the six joints between the base and the rigid top with the bars, being given by

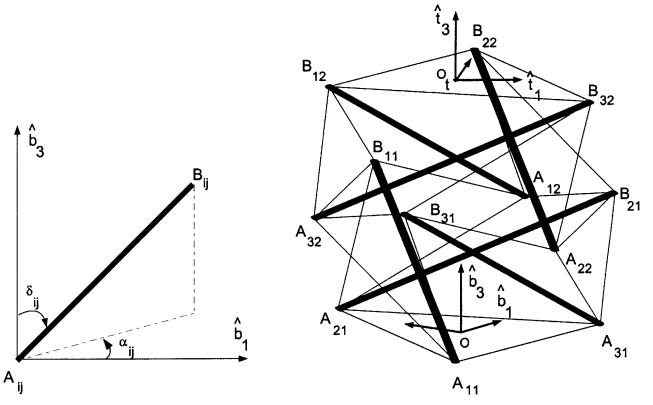

Fig. 2. Two stage SVD tensegrity structure.

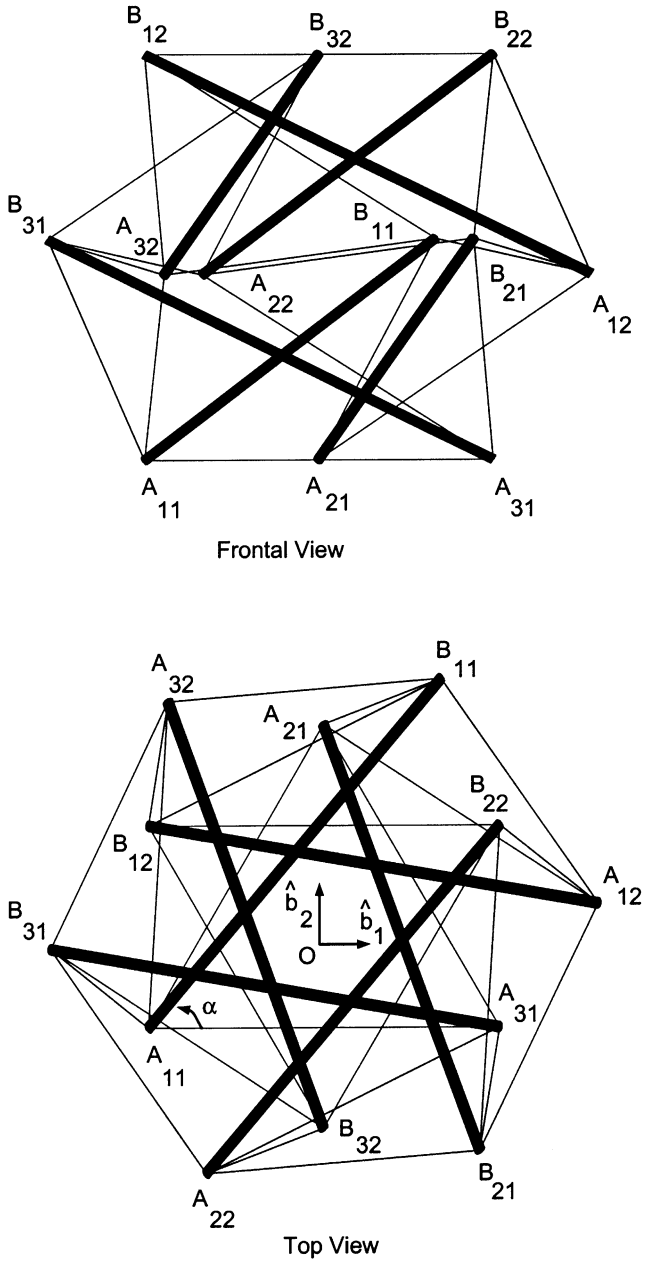

Fig. 3. Symmetrical prestressable configuration.

$$\vec{M}f_j = d_j(\vec{\omega}_a - \vec{\omega}_b),\ j = 1,\ldots,6, \tag{4}$$

where $\vec{M}f_j$, is the friction torque exerted by body 'b' on body 'a' due to the relative angular motion between bodies 'a' and 'b' (in our case 'a' is the base or the rigid top and 'b' is one of the bars). The scalar $d_j \leq 0$ is the coefficient of friction at joint j while $\vec{\omega}_*$ is the angular velocity of rigid body '*'. We neglect the forces exerted on the structure by external force fields (e.g. gravitational). A force and a torque act on the rigid top. We remark that these assumptions are particular cases of the modeling assumptions made for the derivation of tensegrity structures nonlinear and linearized equations of motion. Thus these equations for two stage SVD tensegrity structures have the form given by Eqs. (1) and (3) respectively.

The *inertial* system of reference, $\hat{b}_1$, $\hat{b}_2$, $\hat{b}_3$, is a dextral set of unit vectors, whose center coincides with the geometric center of triangle $A_{11}A_{21}A_{31}$. The axis $\hat{b}_3$ is orthogonal to $A_{11}A_{21}A_{31}$ pointing upward while $\hat{b}_1$ is parallel to $A_{11}A_{31}$, pointing towards A_{31}. The *top's* dextral reference frame, $\hat{t}_1$, $\hat{t}_2$, $\hat{t}_3$, is located at the geometric center of triangle $B_{12}B_{22}B_{32}$, labeled O_t, while $\hat{t}_3$ is orthogonal to $B_{12}B_{22}B_{32}$ pointing upward and $\hat{t}_1$ is parallel to $B_{12}B_{32}$ pointing towards B_{32}. For simplicity it is assumed that the top reference frame is *central principal* for the top rigid body.

The 18 *independent* generalized coordinates used to describe the motion of this *holonomic* system, are: ψ, ϕ, θ, the Euler angles for a 3 1 2 sequence to characterize the inertial orientation of the top reference frame, X, Y, Z, the inertial Cartesian coordinates of the origin of the top reference frame (O_t), δ_{ij} and α_{ij}, the declination and the azimuth of the longitudinal axis of symmetry of bar $A_{ij}B_{ij}$, measured with respect to the inertial frame and defined as follows: δ_{ij} is the angle made by vector $\vec{A_{ij}B_{ij}}$ with $\hat{b}_3$ and α_{ij} is the angle made by the projection of this vector onto plane ($\hat{b}_1$, $\hat{b}_2$) with $\hat{b}_1$ (see Fig. 2). The vector of generalized coordinates is

$$q = [\delta_{11}\alpha_{11}\delta_{21}\alpha_{21}\delta_{31}\alpha_{31}\delta_{12}\alpha_{12}\delta_{22}\alpha_{22}\delta_{32}\alpha_{32}\ \psi\ \phi\ \theta\ X\ Y\ Z]^T \tag{5}$$

3.2. Reference solutions: prestressable configurations

In the following we assume that the bars are identical (their length, mass, and transversal moment of inertia being respectively labeled as l, m, and J) and that the base and top triangles are equal equilateral triangles of side length b.

The reference solution, q_e, is a *prestressable configuration*. A prestressable configuration is an equilibrium one for which all tendons are in tension and which occurs under no external forces or torques (hence $F_e = 0$). The prestressability problem consists in finding a prestressable configuration (see Sultan [7]). The particular prestressable configurations we consider here are coined *symmetrical prestressable configurations* for which the tensions in the saddle, vertical, and diagonal tendons are respectively equal. The geometry of such a configuration is characterized as follows: all bars have the *same declination*, δ, the vertical projections of points A_{i2}, B_{i1}, $i = 1,\ldots,3$, onto the base make a *regular hexagon*, and planes $A_{11}A_{21}A_{31}$ and $B_{12}B_{22}B_{32}$ are *parallel* (see Fig. 3). In addition all saddle tendons have the same tension, T_S, all vertical tendons have the same tension, T_V, all diagonal tendons have the same tension, T_D.

We solved the prestressability problem for this class of configurations (see Sultan [7]) and proved that this

set can be parameterized by two quantities: the azimuth of bar $A_{11}B_{11}$, which we call α, and the common declination of the bars, δ, yielding

$$q_e = [\delta\ \alpha\ \delta\ \alpha + \frac{4\pi}{3}\delta\ \alpha + \frac{2\pi}{3}\delta\ \alpha + \frac{2\pi}{3}\delta\ \alpha\ \delta\ \alpha + \frac{4\pi}{3}\ \frac{5\pi}{3}0\ 0\ 0\ 0\ 2l\cos(\delta) - h]^T \quad (6)$$

where

$$h = \begin{cases} \dfrac{\cos(\delta)}{2\sin(\delta)\cos\left(\alpha + \frac{\pi}{6}\right)}\left(-\dfrac{b}{\sqrt{3}} + p + \sqrt{\dfrac{b^2}{3} - 3p^2}\right) & \text{if} \alpha \neq \dfrac{\pi}{3} \\ \dfrac{l\cos(\delta)}{2} & \text{if} \alpha = \dfrac{\pi}{3} \end{cases} \quad (7)$$

with $p = l\sin(\delta)\cos(\alpha + \frac{\pi}{6})$. These solutions exist if and only if α and δ satisfy the following conditions:

$$\frac{\pi}{6} < \alpha < \frac{\pi}{2},\ 0 < \delta < \frac{\pi}{2}, l\sin(\delta)|\cos(\alpha + \frac{\pi}{6})| < \frac{b}{2\sqrt{3}} \text{ and } \sin(\alpha + \frac{\pi}{6}) < \frac{3l\sin(\delta)}{2b}. \quad (8)$$

This set can be represented in the (α, δ, h) space by an equilibrium surface (see Sultan [7] for details).

We also proved that the tensions are completely determined up to a multiplicative positive scalar, P, called the *pretension coefficient* (see Sultan [7]):

$$[T_S T_V T_D]^T = P[T_{0_S} T_{0_V} T_{0_D}]^T \quad (9)$$

Detailed expressions of the basis tensions, T_{0_S}, T_{0_V}, T_{0_D}, are given in Appendix A.

3.3. Linearized equations of motion

The linearized equations of motion around these prestressable configurations are given by Eq. (3):

$$M_e\ddot{\tilde{q}} + C_e\dot{\tilde{q}} + K_e\tilde{q} + B_e u + H_e f = 0 \quad (10)$$

where $\tilde{q} = q - q_e$, $u = l_0 - l_{0e}$, $f = F$ (since $F_e = 0$) and M_e, C_e, K_e, B_e, H_e are the mass, damping, stiffness, control, and disturbance matrices, respectively, at q_e.

For output feedback control, measurement equations are also necessary. We consider that the measurements, z, are the tendons lengths. Through the same linearization procedure, the measurement equations can be written as

$$\tilde{z} = G_e\tilde{q}, \text{ with } G_e[i,j] = \left(\frac{\partial l_i}{\partial q_j}\right)(q_e). \quad (11)$$

Here $\tilde{z} = z - z_e$, z_e is the vector of tendons lengths at q_e, and G_e is the measurement matrix at q_e.

For simplicity we consider that all the damping coefficients have the same value, $d<0$. We also consider that all saddle tendons are identical, of rest-length S_0 and stiffness k_S, that all vertical tendons are identical, of rest-length V_0 and stiffness k_V, that all diagonal tendons are identical, of rest-length D_0 and stiffness k_D. Here we define the stiffness of tendon i, called k_i, as the product between its cross section, A_i, and modulus of elasticity, E_i (hence $k_i = A_iE_i$). In the following M_t denotes the mass of the rigid top and J_1, J_2, J_3 its principal moments of inertia with respect to the top reference frame.

3.3.1. Mass, damping, and disturbance matrices

The *particular* mass, damping, and disturbance matrices (M_e, C_e, and H_e, respectively), are obtained by evaluating the *general* mass, damping, and disturbance matrices ($M(q)$, $C(q)$, $H(q)$ respectively; see Sultan [16] for details on these matrices) at q_e, where q_e has been expressed in terms of α and δ in Eq. (6). This yields:

$$M_e = M_d + \begin{bmatrix} 0 & 0 & 0 \\ 0 & 0 & M_a \\ 0 & M_a^T & 0 \end{bmatrix} \quad (12)$$

where

$$M_d = \text{diag}([\tilde{J}, \tilde{J}s^2(\delta), \tilde{J}, \tilde{J}s^2(\delta), \tilde{J}, \tilde{J}s^2(\delta), \tilde{J}, \tilde{J}s^2(\delta), \tilde{J}, \tilde{J}s^2(\delta), \tilde{J}_3, \tilde{J}_1, \tilde{J}_2, \tilde{M}, \tilde{M}, \tilde{M}]) \quad (13)$$

with

$$\tilde{J} = J + \frac{mb^2}{4}, \tilde{J}_1 = J_1 + \frac{mb^2}{2}, \tilde{J}_2 = J_2 + \frac{mb^2}{2}, \tilde{J}_3 = J_3 + mb^2, \tilde{M} = M_t + 3m. \quad (14)$$

In these formulas we used the following notation: $c(*) = \cos(*)$, $s(*) = \sin(*)$. Matrix M_a is

$$M_a = \frac{ml}{2}\begin{bmatrix} a & -\frac{e}{\sqrt{3}} & e & c(\delta)s(\alpha + \frac{\pi}{6}) & -c(\delta)c(\alpha + \frac{\pi}{6}) & s(\delta) \\ g & 0 & 0 & s(\delta)c(\alpha + \frac{\pi}{6}) & s(\delta)s(\alpha + \frac{\pi}{6}) & 0 \\ a & 2\frac{e}{\sqrt{3}} & 0 & -c(\delta)c(\alpha) & -c(\delta)s(\alpha) & s(\delta) \\ g & 0 & 0 & s(\delta)s(\alpha) & -s(\delta)c(\alpha) & 0 \\ a & -\frac{e}{\sqrt{3}} & -e & c(\delta)c(\alpha + \frac{\pi}{3}) & c(\delta)s(\alpha + \frac{\pi}{3}) & s(\delta) \\ g & 0 & 0 & -s(\delta)s(\alpha + \frac{\pi}{3}) & s(\delta)c(\alpha + \frac{\pi}{3}) & 0 \end{bmatrix} \quad (15)$$

where $a = \frac{b}{\sqrt{3}}c(\delta)c(\alpha + \frac{\pi}{3})$, $e = \frac{b}{2}s(\delta)$, $g = -\frac{b}{\sqrt{3}}s(\delta)s(\alpha + \frac{\pi}{3})$.

The damping matrix, C_e, is

$$C_e = C_d + \begin{bmatrix} 0 & 0 & 0 \\ 0 & 0 & C_a \\ 0 & C_a^T & 0 \end{bmatrix} \tag{16}$$

where

$$C_d = -d\,\mathrm{diag}([1,1,1,1,1,1,1,1,1,1,1,1,3,3,3,0,0,0]) \tag{17}$$

and

$$C_a = -d\begin{bmatrix} 0 & -s(\alpha) & c(\alpha) & 0 & 0 & 0 \\ -1 & 0 & 0 & 0 & 0 & 0 \\ 0 & c(\alpha-\frac{\pi}{6}) & s(\alpha-\frac{\pi}{6}) & 0 & 0 & 0 \\ -1 & 0 & 0 & 0 & 0 & 0 \\ 0 & -c(\alpha+\frac{\pi}{6}) & -s(\alpha+\frac{\pi}{6}) & 0 & 0 & 0 \\ -1 & 0 & 0 & 0 & 0 & 0 \end{bmatrix}. \tag{18}$$

The disturbance matrix, H_e, is

$$H_e = \begin{bmatrix} 0 \\ H_a \end{bmatrix},\ H_a = \begin{bmatrix} 0 & 0 & -1 & 0 & 0 & 0 \\ -1 & 0 & 0 & 0 & 0 & 0 \\ 0 & -1 & 0 & 0 & 0 & 0 \\ 0 & 0 & 0 & -\frac{1}{2} & -\frac{\sqrt{3}}{2} & 0 \\ 0 & 0 & 0 & \frac{\sqrt{3}}{2} & -\frac{1}{2} & 0 \\ 0 & 0 & 0 & 0 & 0 & -1 \end{bmatrix} \tag{19}$$

for the following distribution of external forces and torques: $F = [M_1\,M_2\,M_3\,F_1\,F_2\,F_3]^T$ where M_*/F_*, is the component along the $\hat{t}_*$ axis of the external torque/force acting on the rigid top.

3.3.2. Stiffness matrix

For the derivation of the stiffness matrix, K_e, we consider the potential energy of the structure which, for linear elastic tendons, is

$$U = \sum_{i=1}^{18} \frac{k_i}{2l_{0_i}}(l_i - l_{0_i})^2 = \frac{k_S}{2S_0}\sum_{i=1}^{6}(S_i - S_0)^2 + \frac{k_V}{2V_0}\sum_{i=1}^{6}(V_i - V_0)^2 + \frac{k_D}{2D_0}\sum_{i=1}^{6}(D_i - D_0)^2. \tag{20}$$

Since there are no external forces acting on the structure when it is in equilibrium at q_e ($F_e = 0$), K_e is just the Hessian of the potential energy evaluated at q_e:

$$K_e[j,n] = \left(\frac{\partial^2 U}{\partial q_j \partial q_n}\right)(q_e) = \left(\frac{k_S}{S_0}\sum_{i=1}^{6}\left(\frac{\partial S_i}{\partial q_j}\frac{\partial S_i}{\partial q_n} + (S_i - S_0)\frac{\partial^2 S_i}{\partial q_j \partial q_n}\right) + \frac{k_V}{V_0}\sum_{i=1}^{6}\left(\frac{\partial V_i}{\partial q_j}\frac{\partial V_i}{\partial q_n} + (V_i - V_0)\frac{\partial^2 V_i}{\partial q_j \partial q_n}\right) + \frac{k_D}{D_0}\sum_{i=1}^{6}\left(\frac{\partial D_i}{\partial q_j}\frac{\partial D_i}{\partial q_n} + (D_i - D_0)\frac{\partial^2 D_i}{\partial q_j \partial q_n}\right)\right)(q_e). \tag{21}$$

Using the expressions for the rest-lengths, S_0, V_0, D_0, corresponding to a symmetrical prestressable configuration with equal saddle, vertical, and diagonal tendons tensions respectively, derived by Sultan [7],

$$S_0 = \frac{k_S S}{T_{0_S} P + k_S},\ V_0 = \frac{k_V V}{T_{0_V} P + k_V},\quad D_0 = \frac{k_D D}{T_{0_D} P + k_D}, \tag{22}$$

we obtain

$$K_e[j,n] = k_V K_V[j,n] + k_S K_S[j,n] + k_D K_D[j,n] + P K_P[j,n] \tag{23}$$

where

$$K_S[j,n] = \frac{1}{S}\sum_{i=1}^{6}\left(\frac{\partial S_i}{\partial q_j}\frac{\partial S_i}{\partial q_n}\right)(q_e),$$

$$K_V[j,n] = \frac{1}{V}\sum_{i=1}^{6}\left(\frac{\partial V_i}{\partial q_j}\frac{\partial V_i}{\partial q_n}\right)(q_e), \tag{24}$$

$$K_D[j,n] = \frac{1}{D}\sum_{i=1}^{6}\left(\frac{\partial D_i}{\partial q_j}\frac{\partial D_i}{\partial q_n}\right)(q_e).$$

Here P is the pretension coefficient, S_i, V_i, D_i, $i = 1,\ldots,6$, are the lengths of the saddle, vertical, and diagonal tendons respectively expressed in terms of the generalized coordinates, q, and S, V, D, the values these functions take for $q = q_e$ (S, V, D are given in Appendix B). Matrices K_S, K_V, K_D can be written as:

$$K_S = \frac{1}{S}A_S A_S^T,\ K_V = \frac{1}{V}A_V A_V^T,\ K_D = \frac{1}{D}A_D A_D^T \tag{25}$$

where, for example,

$$A_S[i,j] = \left(\frac{\partial S_j}{\partial q_i}\right)(q_e),\ j = 1,\ldots,6,\ i = 1,\ldots,18. \tag{26}$$

It is important to remark that, since K_S, K_V, and K_D are expressed as the product of a matrix and its transpose and a positive number, they are all positive semidefinite matrices and that the stiffness matrix, K_e, is linear in pretension and the tendons stiffnesses. Matrices A_S, A_V, A_D are too complicated to be given here (see Sultan [16]).

The elements of matrix K_P can be written as:

$$K_P[j,n] = T_{0_S}(K_S[j,n] + \sum_{i=1}^{6}(\frac{\partial^2 S_i}{\partial q_j \partial q_n})(q_e)) + T_{0_V}(K_V[j,n] + \sum_{i=1}^{6}(\frac{\partial^2 V_i}{\partial q_j \partial q_n})(q_e)) + T_{0_D}(K_D[j,n] + \sum_{i=1}^{6}(\frac{\partial^2 D_i}{\partial q_j \partial q_n})(q_e)). \quad (27)$$

This yields:

$$K_P = K_{P_d} + \begin{bmatrix} 0 & K_{P_3}^T & K_{P_1}^T \\ K_{P_3} & 0 & K_{P_2}^T \\ K_{P_1} & K_{P_2} & 0 \end{bmatrix}. \quad (28)$$

See Sultan [16] for detailed expressions of matrices K_{P_d}, K_{P_i}, $i = 1,2,3$.

3.3.3. Control and measurement matrices

The control matrix can be derived from the potential energy as

$$B_e[i,j] = (\frac{\partial^2 U}{\partial q_i \partial l_{0_j}})(q_e) \quad (29)$$

yielding

$$B_e = [B_S B_V B_D] \quad (30)$$

where

$$B_S = -\frac{(k_S + PT_{0_S})^2}{k_S S} A_S,\ B_V = -\frac{(k_V + PT_{0_V})^2}{k_V V} A_V,\ B_D = -\frac{(k_D + PT_{0_D})^2}{k_D D} A_D. \quad (31)$$

We remark that B_e is quadratic in pretension.

If we assume that the measurement vector is

$$z = [S_1 S_2 \ldots S_6 V_1 V_2 \ldots V_6 D_1 D_2 \ldots D_6]^T \quad (32)$$

where S_i, V_i, and D_i denote the length of the ith saddle, vertical, and diagonal tendon, respectively, then the measurement matrix is

$$G_e[i,j] = \frac{\partial l_i}{\partial q_j}(q_e) \Rightarrow G_e = [A_S A_V A_D]^T. \quad (33)$$

Hence G_e depends only on the geometry of the structure.

3.4. Stability and stiffness properties

In the following we analyze some stability and stiffness properties of two stage SVD tensegrity structures yielding symmetrical prestressable configurations with equal tensions in all saddle, vertical, and diagonal tendons respectively.

The general mass matrix, $M(q)$, was derived along with the total kinetic energy of the system, T_{tot}, which is a quadratic positive definite form in $\dot{q}$: $T_{tot} = \frac{1}{2}\dot{q}^T M(q)\dot{q}$ (see Sultan [16] for details on T_{tot} and $M(q)$). Hence M_e, a particular value of $M(q)$, $M_e = M(q_e)$, is positive definite, $M_e > 0$.

We shall prove directly that C_e is semipositive definite, $C_e \geq 0$, through successive application of Schur complements:

$$C_e \geq 0 \Leftrightarrow \begin{bmatrix} -dI_6 & 0 & 0 \\ 0 & -dI_6 & C_a \\ 0 & C_a^T & C_b \end{bmatrix} \geq 0 \Leftrightarrow C_b + \frac{1}{d} C_a^T C_a \geq 0 \quad (34)$$

where

$$C_b = \begin{bmatrix} -3dI_3 & 0 \\ 0 & 0 \end{bmatrix}. \quad (35)$$

Using C_a expression from Eq. (18), Eq. (34) becomes

$$C_b + \frac{1}{d} C_a^T C_a \geq 0 \Leftrightarrow \begin{bmatrix} 3 - \|w\|^2 & v^T w \\ v^T w & 3 - \|v\|^2 \end{bmatrix} \geq 0 \quad (36)$$

where

$$v = [c(\alpha)\ s(\alpha - \frac{\pi}{6})\ s(\alpha + \frac{\pi}{6})],\ w = [s(\alpha) - c(\alpha - \frac{\pi}{6}) - c(\alpha + \frac{\pi}{6})]. \quad (37)$$

Since $3 - \|w\|^2 > 0$, Eq. (36) is equivalent to

$$\|v\|^2 \|w\|^2 - (v^T w)^2 \geq 0 \quad (38)$$

which is the well known Schwartz inequality.

The stiffness matrix is given by

$$K_e = PK_P + k_S K_S + k_V K_V + k_D K_D. \quad (39)$$

As mentioned before, matrices K_S, K_V, and K_D are positive semidefinite. Matrix $k_S K_S + k_V K_V + k_D K_D$ is positive definite on all space except for the kernel of $[A_S\ A_V\ A_D]^T$. Numerous numerical experiments indicated that K_P is positive definite at all symmetrical prestressable configurations with equal saddle, vertical, and diagonal tendons tensions respectively. This has been ascertained as follows: for various values of l, b, α, and δ, we computed the eigenvalues of K_P. In all cases these eigenvalues were strictly greater than 0. For example in Fig. 4 we give the variation of the minimum eigenvalue of K_P with α and δ for $l = 0.4$ m and $b = 0.27$ m over all the aforementioned prestressable configurations. We ascertain that this eigenvalue is strictly greater than zero in the

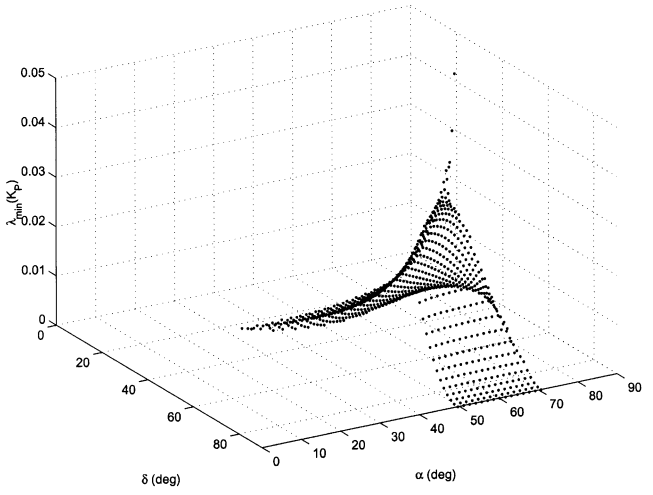

Fig. 4. Minimum eigenvalue of K_P for two stage SVD.

interior of the equilibrium surface. The only points at which this eigenvalue is zero are on one boundary of the equilibrium surface, namely for $\delta = \frac{\pi}{2}$, but these are not feasible prestressable configurations (see Eq. (8): $0 < \delta < \frac{\pi}{2}$).

Thus K_e is positive definite: $K_e > 0$.

These results yield several important consequences:

- $K_e > 0 \Rightarrow \det(K_e) \neq 0$. Since K_e is the Jacobian of $A(q)T(q) + H(q)F$ evaluated at a solution, q_e, of $A(q)T(q) + H(q)F = 0$, by the *implicit function theorem*, it follows that in the neighborhood of each element of the class of symmetrical prestressable configurations with equal tensions in the saddle, vertical, and diagonal tendons respectively, the solution of the static problem, $A(q)T(q) + H(q)F = 0$, can be expressed as a single valued function of the external forces and torques: $q = q(F)$. Hence the static response is well determined (no static bifurcation phenomena are possible).
- $M_e > 0$, $C_e \geq 0$, and $K_e > 0$ imply linearized stability of each symmetrical prestressable configuration with equal saddle, vertical, and diagonal tendons tensions respectively. Actually our numerical experiences indicated that these solutions are asymptotically stable. This fact has been ascertained by applying the following result: a system described by Eq. (3) and for which $M_e > 0$, $K_e > 0$, $C_e \geq 0$ is asymptotically stable if and only if $\text{rank}([\Omega^2 M_e - K_e; C_e]) = \text{rank}(M_e)$ for every natural frequency, Ω, defined by $\det(\Omega^2 M_e - K_e) = 0$ and $\Omega > 0$. We checked the rank of $[\Omega^2 M_e - K_e; C_e]$ for various values of the structure's parameters and over the whole class of prestressable configurations of interest; this rank was always equal to the rank of M_e, $N = 18$. An analytical proof of this fact seems very difficult because of the complicated structure of K_e. This shows that only with kinetic friction at the joints these prestressable configurations are asymptotically stable. We remark that this result is in agreement with the conclusions of Oppenheim and Williams [22,23] obtained for a simpler tensegrity structure and using a different mathematical model, that linear kinetic friction at the joints results in asymptotically stable equilibria, leading to exponential rate of decay of perturbed motions and being more efficient than linear kinetic damping in the tendons.
- $K_P > 0$ shows that the stiffness matrix, K_e, becomes more positive definite if P increases (that is if $P_1 > P_2$ then $K_{e_1} > K_{e_2}$ where P_1 and P_2 are two values of the pretension coefficient and K_{e_*} are the corresponding stiffness matrices). Hence increasing the pretension results in a stiffer structure with higher natural frequencies.

3.5. Linear versus nonlinear dynamics

We next present numerical simulations of a two stage SVD tensegrity structure's linear and nonlinear dynamics. This will help us evaluate the differences between the nonlinear and linear models and the influence of pretension upon these differences.

The structure analyzed here is characterized by the fact that all bars are identical, of length $l = 0.4$ m, mass $m = 0.8$ kg, and transversal moment of inertia $J = 1.2$ kg m^2. The base and top triangles are equal, equilateral triangles of side length $b = 0.27$ m. The coefficients of friction at all joints are equal, $d_i = -4$, $i = 1,\ldots,6$. The mass of the rigid top is $M_t = 10$ kg and its moments of inertia $J_1 = 30$ kg m^2, $J_2 = 40$ kg m^2, $J_3 = 50$ kg m^2. The tendons are assumed to have the same stiffness, $k_i = 500$ N, $i = 1,\ldots,18$.

We consider that the structure is in equilibrium, yielding a symmetrical prestressable configuration for which the tensions in all saddle, all vertical, and all diagonal tendons are respectively equal. This configuration is characterized by:

$$\alpha_{11} = \alpha_{22} = \frac{\pi}{3}, \alpha_{21} = \alpha_{32} = \frac{5\pi}{3},$$

$$\alpha_{31} = \alpha_{12} = \pi, \psi = \frac{5\pi}{3}, \phi = \theta = X = Y = 0, \qquad (40)$$

$$Z = 0.3 \text{ m}, \delta_{ij} = \frac{\pi}{3} \text{ for } i = 1,2,3, j = 1,2,3.$$

For a given pretension coefficient, P, the rest-lengths of the tendons which assure this prestressable configuration can be determined using Eq. (22).

Figs. 5 and 6 represent the responses of the linear and nonlinear models of the structure to a perturbation in the

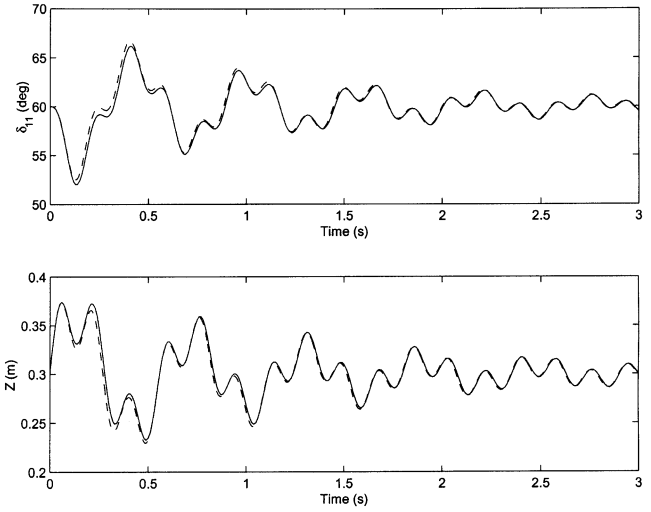

Fig. 5. Initial conditions response for $P = 500$: nonlinear (- - -) and linear models (———).

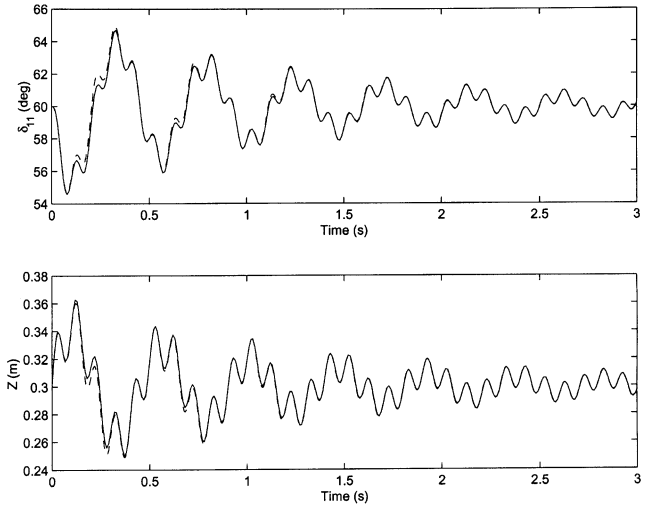

Fig. 6. Initial conditions response for $P = 2500$: nonlinear (- - -) and linear models (———).

initial conditions. The perturbation consists of a vertical velocity of the rigid top equal to $2\ \mathrm{m\ s^{-1}}$: $\dot{Z}(0) = 2\ \mathrm{m\ s^{-1}}$. These graphs represent time histories of three generalized coordinates (δ_{11}, α_{11}, and Z). Fig. 5 corresponds to the case of a pretension coefficient of $P = 500$, while Fig. 6 corresponds to $P = 2500$. The time histories of the other generalized coordinates and generalized velocities are *qualitatively* similar. We have also checked that the tendons are always in tension and that the bars do not collide with each other throughout the motion.

These simulations illustrate the differences between the nonlinear and linear models. We ascertain that the pretension coefficient increases the frequencies of the linear response (the higher the pretension coefficient the higher these frequencies are). We also note that at higher pretension the differences between the linear and nonlinear models are less significant. Hence the linear approximation is better at high pretension. We also note that the same differences are more significant at high generalized velocities. This is so because of the quadratic terms in generalized velocities which appear in the nonlinear model, $c = c(q,\dot{q})$, but do not appear in the linear model. We also note that these responses are typical of an asymptotically stable equilibrium: the motion dies out in time and settles down to the unperturbed equilibrium state.

The same conclusions are reached if we consider different initial conditions perturbations and different reference solutions in the class of symmetrical prestressable configurations with equal tensions in all saddle, all vertical, and all diagonal tendons respectively.

3.6. Dynamic characteristics

In the following we investigate the dynamic characteristics of a two stage SVD tensegrity structure yielding symmetrical prestressable configurations with equal saddle, vertical, and diagonal tendons tensions respectively.

Consider a two stage SVD tensegrity structure having the following geometrical, inertial, and elastic characteristics: $l = 0.4$ m, $b = 0.27$ m, $m = 0.8$ kg, $J = 1.2$ kg m^2, $M_t = 10$ kg, $J_1 = 30$ kg m^2, $J_2 = 40$ kg m^2, $J_3 = 50$ kg m^2, $k_i = 500$ N, $i = 1,\ldots,18$. The pretension is $P = 500$. The natural frequencies of a system whose linearized dynamics is described by Eq. (10) are defined by the square roots of the eigenvalues of the matrix $M_e^{-1}K_e$. The variations of the minimum and maximum natural frequencies of this structure over the whole class of symmetrical prestressable configurations of interest are given in Figs. 7 and 8. We ascertain that the dynamic range (defined as the difference between the maximum natural frequency and the minimum one) increases for

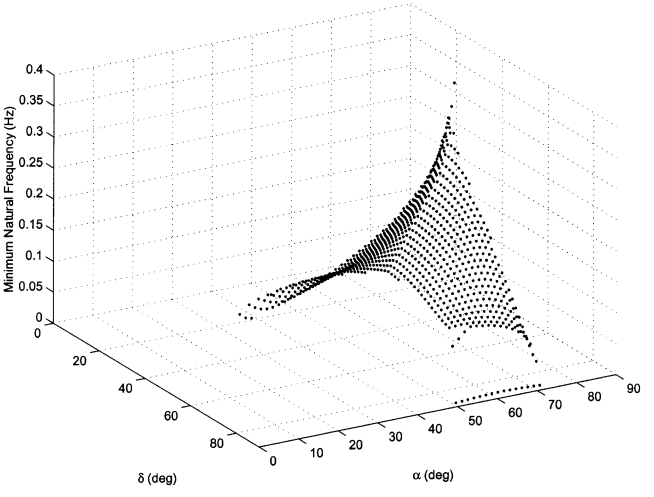

Fig. 7. Minimum natural frequency for two stage SVD.

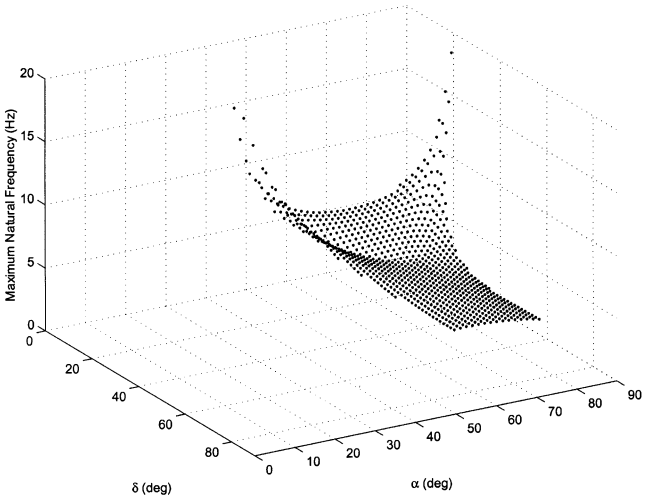

Fig. 8. Maximum natural frequency for two stage SVD.

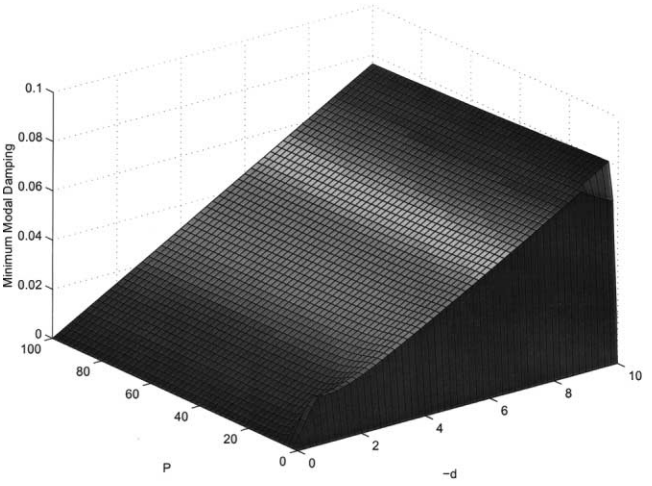

Fig. 9. Minimum modal damping for two stage SVD.

small declination (δ) because of the dramatic increase of the maximum natural frequency.

It is also interesting to evaluate the influence of the damping and pretension coefficients on the dynamic characteristics of the structure by plotting the minimum and maximum modal dampings and the minimum and maximum modal frequencies of the structure over the damping and pretension coefficients. Recall that for a first order linear system whose dynamics is described by

$$\dot{x} = A_p x + B_p u + H_p f \tag{41}$$

the modal dampings and the modal frequencies are defined by the eigenvalues of the system matrix, A_p: the absolute value of the real part of an eigenvalue is the modal damping whereas the absolute value of the imaginary part is the modal frequency. We can easily cast our vector second order system given by Eq. (10) in first order form by introducing the vector of state variables $x = [\tilde{q}^T \dot{\tilde{q}}^T]^T$. Hence

$$A_p = \begin{bmatrix} 0 & I \\ -M_e^{-1}K_e & -M_e^{-1}C_e \end{bmatrix}, \tag{42}$$

$$B_p = \begin{bmatrix} 0 \\ -M_e^{-1}B_e \end{bmatrix}, \; H_p = \begin{bmatrix} 0 \\ -M_e^{-1}H_e \end{bmatrix}.$$

Consider a two stage SVD tensegrity structure whose geometrical, inertial, and elastic characteristics are the same as before and which yields a symmetrical prestressable configuration for which the tensions in the saddle, vertical, and diagonal tendons are respectively equal and characterized by $\alpha = \frac{\pi}{3}$ and $\delta = \frac{\pi}{3}$. The variations of the minimum and maximum modal dampings with the pretension and damping coefficients for this configuration are given in Figs. 9 and 10 and those of the minimum and maximum modal frequencies in Figs. 11 and 12 respectively. As expected, the minimum and maximum

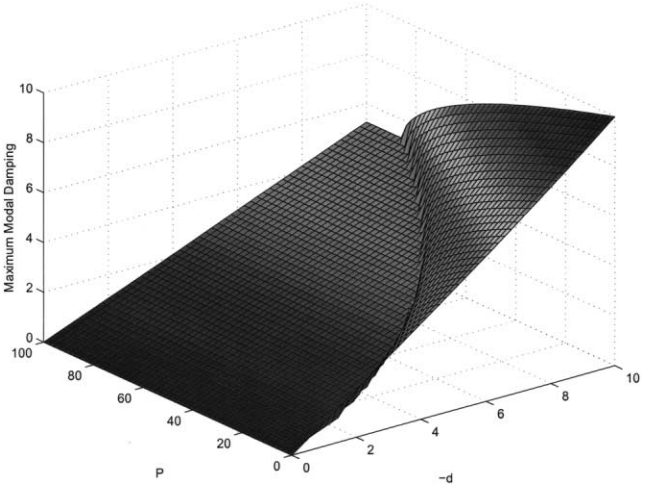

Fig. 10. Maximum modal damping for two stage SVD.

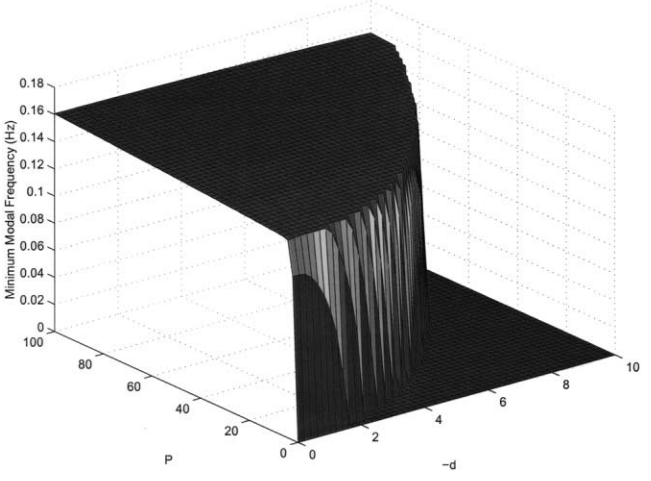

Fig. 11. Minimum modal frequency for two stage SVD.

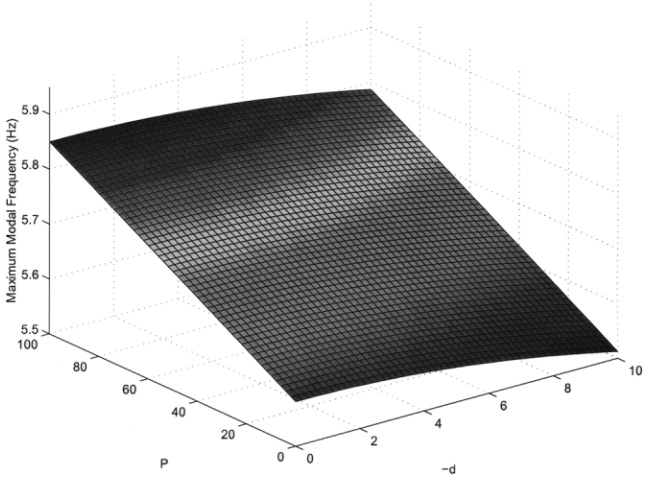

Fig. 12. Maximum modal frequency for two stage SVD.

modal dampings increase with the damping. It is interesting to remark that, for a given damping coefficient, at small pretension the maximum modal damping increases as the pretension decreases. We also remark that the range of modal damping (defined as the difference between the maximum modal damping and the minimum one) increases as the damping in the structure increases. Also the modal dynamic range (defined as the difference between the maximum modal frequency and the minimum one) increases with the pretension coefficient.

It is worth mentioning that for *some* combination of damping and pretension the minimum modal frequency is zero (Fig. 11). This means that some modes of the linear system are pure exponentially decaying ones (of the type $\exp(-\zeta t)$, ζ being the modal damping and t the time). Also, since the maximum modal damping is greater than zero for any combination of damping and pretension in the range under investigation (Fig. 12), there are always exist oscillatory modes whose envelope is exponentially decaying (of the type $\exp(-\zeta t)\cos(\omega t)$), ω being the modal frequency).

4. Two stage SVDT tensegrity structures

In the following we analyze another class of tensegrity structures, coined two stage SVDT. A two stage SVDT tensegrity structure is obtained from a SVD one if we replace the top rigid body with tendons connecting the top nodal points, B_{12}, B_{22}, and B_{32}. These new tendons—$B_{12}B_{22}$, $B_{22}B_{32}$, $B_{32}B_{12}$—will be called *top* tendons, hence the acronym 'SVDT' used for these structures.

We make the same modeling assumptions as for two stage SVD tensegrity structures and we define the inertial reference frame in the same way. The independent generalized coordinates used to describe this system's configuration are the Cartesian coordinates, x_{i2}, y_{i2}, z_{i2}, of the mass center of bar $A_{i2}B_{i2}$, $i = 1,2,3$, with respect to the inertial reference frame, the azimuth α_{ij} and the declination δ_{ij}, which characterize the orientation of bar $A_{ij}B_{ij}$, $i = 1,2,3$, $j = 1,2$, with respect to the inertial frame (these angles are defined in the same way as the declination and azimuth used for two stage SVD tensegrity structures). The vector of generalized coordinates is:

$$q = [\delta_{11}\alpha_{11}\delta_{21}\alpha_{21}\delta_{31}\alpha_{31}x_{12}y_{12}z_{12}\delta_{12} \quad \alpha_{12}x_{22}y_{22}z_{22}\delta_{22}\alpha_{22}x_{32}y_{32}z_{32}\delta_{32}\alpha_{32}]^T. \tag{43}$$

4.1. Reference solutions

In the following, as in the SVD case, we consider that all bars have the same length, l, mass, m, and transversal moment of inertia, J. The reference solutions are symmetrical prestressable configurations for which the tensions in the saddle, vertical, diagonal, and top tendons are respectively equal. The geometry of these configurations is identical to that of the symmetrical prestressable configurations of the two stage SVD tensegrity structures previously investigated. It has been proved by Sultan [7] that the solution of the prestressability problem for these configurations is given by:

$$\begin{aligned}
&\alpha_{11} = \alpha_{22} = \alpha,\ \alpha_{21} = \alpha_{32} = \alpha + \frac{4\pi}{3},\ \alpha_{31} \\
&= \alpha_{12} = \alpha + \frac{2\pi}{3},\ x_{12} = \frac{l}{4}\sin(\delta)\cos(\alpha) \\
&+ \frac{\sqrt{3}}{4}l\sin(\delta)\sin(\alpha) - \frac{b}{2},\ y_{12} = \frac{b}{2\sqrt{3}} \\
&- \frac{\sqrt{3}}{4}l\sin(\delta)\cos(\alpha) + \frac{l}{4}\sin(\delta)\sin(\alpha),\ z_{12} \\
&= \frac{3}{2}l\cos(\delta) - h,\ x_{22} = \frac{b}{2} - \frac{l}{2}\sin(\delta)\cos(\alpha),\ y_{22} \\
&= \frac{b}{2\sqrt{3}} - \frac{l}{2}\sin(\delta)\sin(\alpha),\ z_{22} = \frac{3}{2}l\cos(\delta) - h,\ x_{32} \\
&= \frac{l}{4}\sin(\delta)\cos(\alpha) - \frac{\sqrt{3}}{4}l\sin(\delta)\sin(\alpha),\ y_{32} \\
&= \frac{l}{4}\sin(\delta)\sin(\alpha) + \frac{\sqrt{3}}{4}l\sin(\delta)\cos(\alpha) - \frac{b}{\sqrt{3}},\ z_{32} \\
&= \frac{3}{2}l\cos(\delta) - h,\ \delta_{ij} = \delta,\ i = 1,2,3,\ j = 1,2,
\end{aligned} \tag{44}$$

where h is given by the same formula as in the SVD case (Eq. (7)) and b represents the length of the base and top triangles side (these triangles are equilateral at the prestressable configurations considered here). This

set is identical with the set of symmetrical prestressable configurations with equal tensions in the saddle, vertical, and diagonal tendons, respectively, of two stage SVD tensegrity structures (see Sultan [7] for the proof).

We have also proved that the tensions at these configurations are completely determined up to a multiplicative, positive, scalar (see Sultan [7]):

$$[T_S T_V T_D T_T]^T = P[T_{0_S} T_{0_V} T_{0_D} T_{0_T}]^T \tag{45}$$

where P is the pretension coefficient, T_S, T_V, T_D, T_T are the tensions in the saddle, vertical, diagonal, and top tendons respectively, and T_{0_S}, T_{0_V}, T_{0_D}, T_{0_T} are given in Appendix C.

4.2. Linearized equations of motion

The linearized equations of motion around the aforementioned reference solutions are given by Eq. (3):

$$M_e \ddot{\tilde{q}} + C_e \dot{\tilde{q}} + K_e \tilde{q} + B_e u + H_e f = 0 \tag{46}$$

For simplicity, we shall not consider the case of external disturbances in the following (hence $F = F_e = f = 0$) and we shall not be interested in the disturbance matrix, H_e. The controls are assumed to be the rest-lengths of the tendons. As in the SVD case we also consider that all the damping coefficients have the same value, $d<0$, all saddle tendons are identical, of rest-length S_0 and stiffness k_S, all vertical tendons are identical, of rest-length V_0 and stiffness k_V, all diagonal tendons are identical, of rest-length D_0 and stiffness k_D, and all top tendons are identical, of rest-length T_0 and stiffness k_T.

4.2.1. Linearized equations of motion matrices

The mass matrix is diagonal:

$$M_e = \text{diag}([J + \frac{ml^2}{4}, (J + \frac{ml^2}{4})s^2(\delta), J + \frac{ml^2}{4}, \tag{47}$$

$$(J + \frac{ml^2}{4})s^2(\delta), J + \frac{ml^2}{4}, (J + \frac{ml^2}{4})s^2(\delta),$$

$$m,m,m,J,Js^2(\delta),m,m,m,J,Js^2(\delta),m,m,m,J,Js^2(\delta)]).$$

The damping matrix is also diagonal:

$$C_e = \tag{48}$$

$$-d\text{diag}([1,1,1,1,1,1,0,0,0,0,0,0,0,0,0,0,0,0,0,0,0])$$

The stiffness matrix can be derived from the potential energy as in the SVD case yielding

$$K_e = PK_P + k_S K_S + k_V K_V + k_D K_D + k_T K_T. \tag{49}$$

where matrices K_P, K_S, K_V, K_D, K_T are given by similar formulas as in the SVD case (see Eqs. (24) and (27)).

Analogously, the control matrix is

$$B_e = [B_S B_V B_D B_T] \tag{50}$$

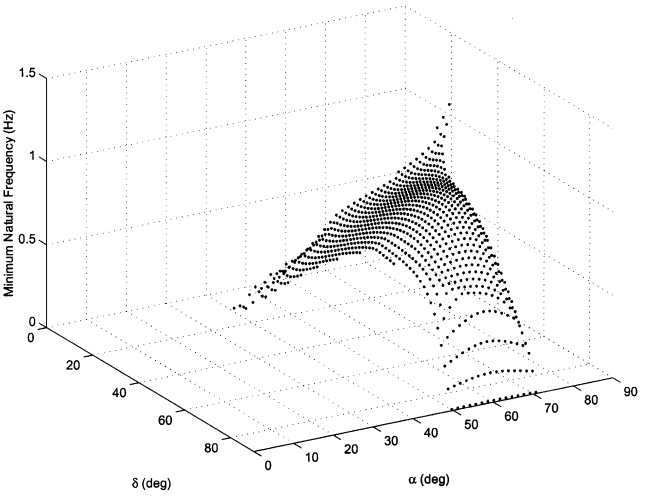

Fig. 13. Minimum natural frequency for two stage SVDT.

where B_S, B_V, B_D, B_T are given by similar formulas as in the SVD case (see Eq. (31)), hence B_e is quadratic in pretension.

It is important to remark that these results, regarding the structure of the stiffness and control matrices at prestressable configurations, can be easily generalized to other tensegrity structures characterized by the modeling assumptions stated in this article. Namely *the stiffness matrix is linear* in the level of pretension and the tendons stiffnesses whereas *the control matrix is quadratic* in pretension.

4.3. Stability properties and dynamic characteristics

It is easy to observe that at these prestressable configurations the mass matrix is positive definite whereas the damping one is semipositive definite: $M_e > 0$, $C_e \geq 0$ (since $0 < \delta < \frac{\pi}{2}$). It has also been numerically ascer-

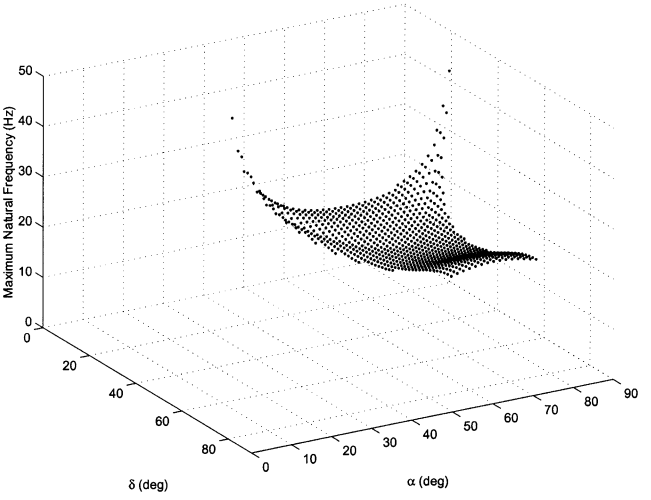

Fig. 14. Maximum natural frequency for two stage SVDT.

tained (similarly with the SVD case) that $K_P>0$. Hence $K_e>0$, implying, as in the SVD case, stability of these configurations. Actually all our numerical experiments indicated that these are asymptotically stable equilibrium configurations.

Figs. 13 and 14 show the variations of the minimum and maximum natural frequencies with α and δ over the whole class of symmetrical prestressable configurations with equal tensions in the saddle, vertical, diagonal, and top tendons respectively for a two stage SVDT tensegrity structure with the following parameters: $l = 0.4$ m, $b = 0.27$ m, $m = 0.8$ kg, $J = 1.2$ kg m^2, $P = 500$, $k_S = k_V = k_D = k_T = 500$ N. As in the SVD case, we ascertain how the dynamic range dramatically increases as δ decreases.

The influence of pretension and damping on the same structure at a symmetrical prestressable configuration with equal saddle, vertical, diagonal, and top tendons tensions, respectively, characterized by $\alpha = \frac{\pi}{3}$ and $\delta = \frac{\pi}{3}$ is also evaluated. The variations of the minimum and maximum modal dampings with the pretension and damping coefficients are plotted in Figs. 15 and 16. We observe that the range of the modal damping increases with the damping in the structure. The minimum and maximum modal frequencies variations with the pretension and damping coefficients are given in Figs. 17 and 18. As in the SVD case, the modal dynamic range increases with the level of pretension. We also remark that the maximum modal frequency is greater than zero, leading to the existence of oscillatory modes whose envelope is exponentially decaying, and that, for some combination of damping and pretension, the minimum modal frequency is zero, leading to the existence of pure exponentially decaying modes (see Figs. 17 and 18).

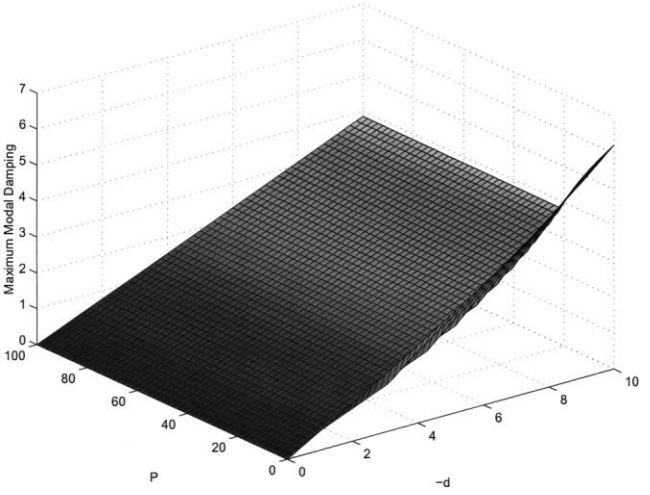

Fig. 16. Maximum modal damping for two stage SVDT.

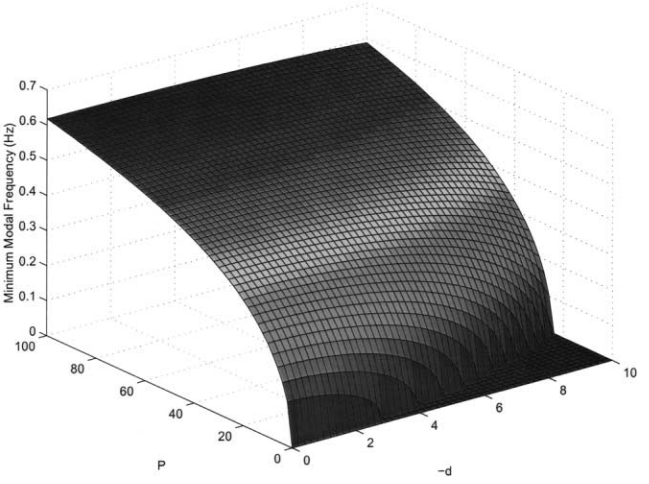

Fig. 17. Minimum modal frequency for two stage SVDT.

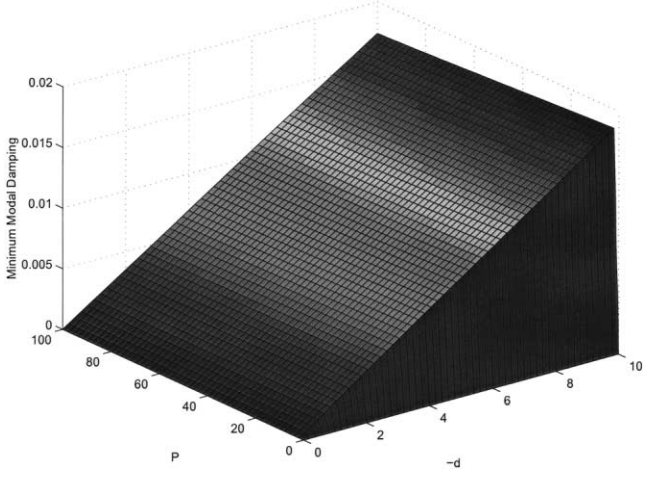

Fig. 15. Minimum modal damping for two stage SVDT.

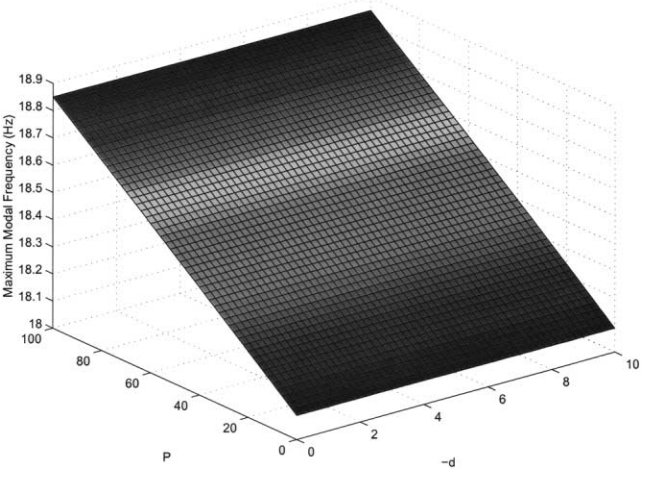

Fig. 18. Maximum modal frequency for two stage SVDT.

5. Conclusions

Linear models which describe the approximate dynamics of tensegrity structures in the neighborhood of equilibrium reference solutions have been derived. For two classes of tensegrity structures these equations have been presented. The reference solutions around which these linear models are built are prestressable configurations of practical interest. The stiffness matrix at these configurations is linear in the level of pretension and the tendons stiffnesses whereas the control matrix is quadratic in pretension. The mass and stiffness matrices are positive definite and the damping matrix is positive semidefinite. Hence these reference solutions are stable. Numerical experiences indicated that they are actually asymptotically stable, showing that only linear kinetic friction at the rigid to rigid joints is sufficient to assure asymptotical stability of these configurations. The modal dynamic range generally increases with the pretension whereas the modal damping range increases with the damping.

Appendix A

Two stage SVD tensegrity structures basis tensions are:

$$[T_{0_S} T_{0_V} T_{0_D}] = \frac{[T_S^r T_V^r T_D^r]}{\sqrt{6}\|[T_S^r T_V^r T_D^r]\|} \tag{51}$$

where

$$T_V = \begin{cases} \frac{V}{D}\frac{1}{\sqrt{3}\cos(\alpha+\frac{\pi}{6})}\left(\left(\frac{l\cos(\delta)}{h}-1\right)\sin\left(\alpha-\frac{\pi}{6}\right)-\cos(\alpha)\right)T_D & \text{if} \alpha \neq \frac{\pi}{3} \\ \frac{VT_D}{D}\left(\frac{3l}{2b}\sin(\delta)-1\right) & \text{if} \alpha = \frac{\pi}{3}, \end{cases} \tag{52}$$

$$T_S^r = \begin{cases} \frac{S}{D}\left(\frac{l\cos(\delta)}{h}-1\right)T_D^r & \text{if } \alpha \neq \frac{\pi}{3} \\ T_D^r & \text{if } \alpha = \frac{\pi}{3}, \end{cases} \tag{53}$$

$$T_D^r = 1. \tag{54}$$

Appendix B

Saddle, vertical, and diagonal tendons lengths at symmetrical prestressable configurations:

$$S = \sqrt{h^2 + \frac{b^2}{3} + l^2\sin^2(\delta) - \frac{2}{\sqrt{3}}lb\sin(\delta)\cos(\alpha-\frac{\pi}{6})}, \tag{55}$$

$$V = \sqrt{b^2 + l^2 - 2lb\sin(\delta)\sin(\alpha+\frac{\pi}{6})}, \tag{56}$$

$$D = \sqrt{h^2 + \frac{b^2}{3} + l^2 - \frac{2}{\sqrt{3}}lb\sin(\delta)\sin(\alpha) - 2lh\cos(\delta)}. \tag{57}$$

Appendix C

Two stage SVDT tensegrity structures basis tensions are:

$$[T_{0_S} T_{0_V} T_{0_D} T_{0_T}] = \frac{[T_S^r T_V^r T_D^r T_T^r]}{\sqrt{6}\|[T_S^r T_V^r T_D^r \sqrt{0.5} T_T^r]\|} \tag{58}$$

where T_V^r, T_S^r, and T_D^r are given by Eqs. (52)–(54) whereas T_T^r is

$$T_T^r = \tag{59}$$

$$\begin{cases} 3l^2\sin(\delta)\cos(\delta) + 6bh\cos\left(\alpha-\frac{\pi}{3}\right) \\ \frac{T_D^r}{6D}\ \frac{-6lh\sin(\delta)-2\sqrt{3}bl\cos(\delta)\sin(\alpha)}{\sqrt{3}h\cos\left(\alpha+\frac{\pi}{6}\right)} \quad \text{if } \alpha \neq \frac{\pi}{3} \\ \frac{T_D^r}{6D}\ \frac{2b^2-9lb\sin(\delta)+9l^2\sin^2(\delta)}{b} \quad \text{if } \alpha = \frac{\pi}{3}. \end{cases}$$

References

[1] Pugh A. An introduction to tensegrity. Berkeley, CA: University of California Press, 1976.

[2] Calladine CR. Buckminster Fuller's tensegrity structures and Clerk Maxwell's rules for the construction of stiff frames. Int J Solids Struct 1978;14:161–72.

[3] Pellegrino S, Calladine CR. Matrix analysis of statically and kinematically indetermined frameworks. Int J Solids Struct 1986;22(4):409–28.

[4] Connelly R, Whiteley W. Second order rigidity and prestress stability for tensegrity frameworks. SIAM J Discr Math 1996;9:453–91.

[5] Skelton RE, Sultan C. Controllable tensegrity, a new glass of smart structures. In: Proceedings of the SPIE 4th Symposium on Smart Structures and Materials vol. 3039, 1997, pp. 166–77.

[6] Sultan C, Corless M, Skelton RE. A tensegrity flight simulator. J Guid Contr Dynam 2000;23(6):1055–64.

[7] Sultan C, Corless M, Skelton RE. The prestressability problem of tensegrity structures. Some analytical solutions. Int J Solids Struct 2001;38(30–31):5223–52.

[8] Pellegrino S. Analysis of prestressed mechanisms. Int J Solids Struct 1990;26(12):1329–50.

[9] Calladine CR. Modal stiffness of a pretensioned cable net. Int J Solids Struct 1982;18:829–46.

[10] Calladine CR, Pellegrino S. First order infinitesimal mechanisms. Int J Solids Struct 1991;27:505–15.

[11] Motro R, Najari S, Jouanna P. Static and dynamic analysis of tensegrity systems. In: Proceedings of the ASCE International Symposium. New York: Springer-Verlag; 1986.

[12] Motro R. Tensegrity systems and geodesic domes. Int J Space Struct 1990;5(3):343–54.
[13] Motro R. Tensegrity systems: the state of the art. Int J Space Struct 1992;7(2):75–83.
[14] Hanaor A. Prestressed pin-jointed structures—flexibility analysis and prestress design. Comput Struct 1988;28(6):757–69.
[15] Hanaor A. Aspects of design of double layer tensegrity domes. Int J Space Struct 1992;7(2):101–13.
[16] Sultan C. Modeling, design, and control of tensegrity structures with applications, Ph.D. dissertation, Purdue University, West Lafayette, 1999.
[17] Sultan C, Corless M, Skelton RE. Reduced prestressability conditions for tensegrity structures. In Proceedings of AIAA/ASME/ASCE/AHS/ASC 40th Structures, Structural Dynamics and Materials Conference, AIAA-99-1478, 12–15 April, St Louis, USA, 1999, pp. 2300–8.
[18] Furuya H. Concept of deployable tensegrity structures in space application. Int J Space Struct 1992;7(2):143–51.
[19] Murakami H. Static and dynamic analyses of tensegrity structures. Part 1: nonlinear equations of motion. Int J Solids Struct 2001;38:3599–613.
[20] Murakami H. Initial shape finding and modal analyses of cyclic right-cylindrical tensegrity modules. Comput Struct 2001;79:891–917.
[21] Murakami H. Static and dynamic characterization of some tensegrity structures. ASME J Appl Mech 2001;68:19–27.
[22] Oppenheim IJ, Williams WO. Vibration of an elastic tensegrity structure. European Journal of Mechanics A/solids 2001;20(6):1023–31.
[23] Oppenheim IJ, Williams WO. Vibration and damping in 3 hour tensegrity structures. ASCE J Aerospace Engng 2001;14(3):85–91.
[24] Djouadi S, Motro R, Pons JC, Crosnier B. Active control of tensegrity systems. ASCE J Aerospace Engng 1998;11(2):37–44.
[25] Sultan C, Skelton RE. Integrated design of controllable tensegrity structures. In: Proceedings of the ASME Congress Exposition vol. 54, 1997, pp. 27–37.
[26] Sultan C, Corless M, Skelton RE. Nonlinear robust tracking control of a tensegrity motion simulator. In: Proceedings of the SPIE 12th Intl Conference on Sensing, Simulation and Control vol. 365,1998, pp. 179–90.
[27] Sultan C, Skelton RE. Tendon control deployment of tensegrity structures. In: Proceedings of the SPIE 5th Symposium on Smart Structures and Materials, vol. 3323,1998, pp. 455–66.
[28] Sultan C, Skelton RE. Force and torque smart tensegrity sensor. In: Proceedings of the SPIE 5th Symposium on Smart Structures and Materials, vol. 3323, 1998, pp. 357–68.
[29] Sultan C, Corless M, Skelton RE. Peak to peak control of an adaptive tensegrity space telescope. In: Proceedings of the SPIE 6th Symposium on Smart Structures and Materials, vol. 3667, 1999, 190–201.